Directional Bremsstrahlung from a Ti Laser-Produced X-Ray Source at Relativistic Intensities in the 3–12 keV Range

F. Zamponi,[1,*,†] A. Lübcke,[1,*] T. Kämpfer,[1] I. Uschmann,[1] E. Förster,[1] A. P. L. Robinson,[2] A. Giulietti,[3,4] P. Köster,[3,4] L. Labate,[3,4] T. Levato,[3,4,‡] and L. A. Gizzi[3,4]

[1]*Institut für Optik und Quantenelektronik, Friedrich-Schiller-Universität Jena, Max-Wien-Platz 1, 07743 Jena, Germany*
[2]*Central Laser Facility, STFC Rutherford-Appleton Laboratory, Chilton, OX11 0QX, United Kingdom*
[3]*ILIL, Istituto Nazionale di Ottica, UOS "Adriano Gozzini," CNR, Via G. Moruzzi 1, Pisa, Italy*
[4]*INFN, Sezione di Pisa, Largo B. Pontecorvo 3, Pisa, Italy*

(Received 24 December 2008; revised manuscript received 12 May 2010; published 16 August 2010)

Front and rear side x-ray emission from thin titanium foils irradiated by ultraintense laser pulses at intensities up to $\approx 5 \times 10^{19}$ W/cm^2 was measured using a high-resolution imaging system. Significant differences in intensity, dimension, and spectrum between front and rear side emission intensity in the 3–12 keV photon energy range was found even for 5 μm thin Ti foils. Simulations and analysis of space-resolved spectra explain this behavior in terms of directional bremsstrahlung emission from fast electrons generated during the interaction process.

DOI: 10.1103/PhysRevLett.105.085001 PACS numbers: 52.38.Ph, 52.70.La

Electrons accelerated by the interaction between an ultrashort laser pulse and a plasma and injected in a cold target create x rays via bremsstrahlung and K-shell ionization [1,2]. There are many features that make such a source appealing [3]. The x-ray burst is very bright (up to 10^{12} Ti-$K\alpha$ photons per pulse can be produced [4]), the expected duration is 100–600 fs, depending on the material, target thickness, and laser intensity [5–7], and the source has a size, for lower laser intensities, comparable to the laser focal spot size [8,9].

$K\alpha$ emission is also used to monitor the fast electron behavior in matter. A typical experimental configuration for this class of experiments is based upon the use of layered targets, where layers characterized by different atomic species are used as fluorescence tracers for the fast electron beam [10–14].

In this work we focus our attention to the emission of such an x-ray source created by an ultraintense laser pulse by means of a high-resolution x-ray imaging system capable of spectral analysis.

The experiment was performed at the JeTi, multi-TW Ti:sapphire laser system in Jena. The experimental setup is sketched in Fig. 1. The laser pulse was tightly focused to about 5 μm^2 to reach intensities ranging from 1.5×10^{19} W/cm^2 to 5×10^{19} W/cm^2 by varying the energy, up to about 500 mJ on target. To avoid plasma production by the laser before the arrival of the main pulse, amplified spontaneous emission and prepulses were reduced by a fast Pockels cell. The target consisted of Ti foil with either 5 or 25 μm thickness. Two x-ray pinhole cameras, equipped with 5 μm diameter pinholes with two well-characterized identical CCD cameras having identical sensitivity within 1% [15], imaged the front and the rear side of the target from an angle of view of 45° with respect to the target normal. The spatial resolution of the imaging system was about 5 μm on target with a magnification $M = 11$. The CCD cameras were made blind for visible and infrared radiation by using filters. Because of the used x-ray filters and the CCD sensitivity, the spectra were recorded in the range of 3–12 keV.

The images of Fig. 2 show a comparison between front and rear side x-ray images acquired in consecutive shots and taken at two different target thicknesses (5 and 25 μm). A comparison between images taken at two different laser intensities (lower intensity: 1.5×10^{19} W/cm^2 and higher intensity 5×10^{19} W/cm^2) for the 25 μm thick targets is also shown. In the final sum image (4 series), in order to compensate for possible shot-to-shot variations of the source position, single images were aligned with respect to their center of mass. The values of the FWHMs were obtained by making vertical lineouts of the images: in this way, the distortion due to the observation direction (45° in the horizontal plane) plays no role.

The images are shown as they were detected on the CCD; no compensation for the 45° observation angle was done. In fact, while for the 5 μm target this is a simple

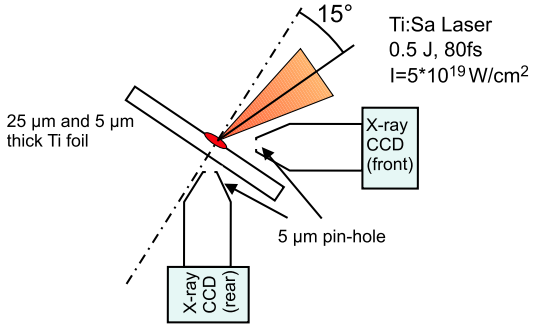

FIG. 1 (color online). Experimental setup.

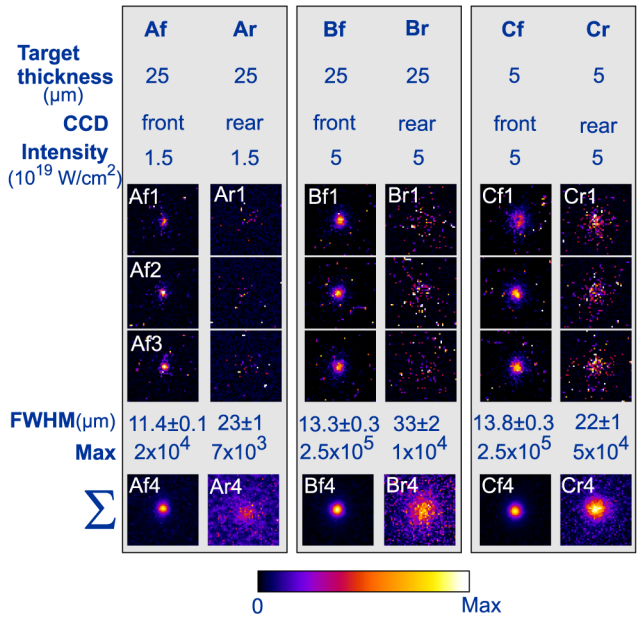

FIG. 2 (color online). X-ray images of the source obtained from a series of consecutive single laser pulses (from 1 to 3 for the three columns. The "f" refers to front CCD, "r" to rear CCD). For each column a different intensity scale was used. The size of the images is 120 μm $\times$ 170 μm on the target plane. The difference is due to the 45° angle of view. The series are organized in three different groups. In each group the irradiation conditions for the two columns are the same, however one column shows the front side source, the other one the rear side source. Images of the same group in the same row concern the very same laser pulses as seen from the two cameras. Images $Af4$ to $Cr4$: sum of about 110 images with the above described characteristics. The FWHMs of the vertical lineouts refer to the sum images (4 series).

task, for the 25 μm target, the source dimension is comparable to the target thickness and contribution of the emission from the deeper target regions must be taken into account.

We first compare the front images taken at the same laser intensity for two target thicknesses, namely, $Bf4$ and $Cf4$. These images give similar source sizes: 13.3 μm and 13.8 μm for the 5 μm and the 25 μm target, respectively. In contrast, the size of the x-ray source seen in the corresponding rear images, $Br4$ and $Cr4$, is much different for the two thicknesses, namely 21.3 μm for the 5 μm target and 33 μm for the 25 μm target. According to these results, the size of the source seen from the rear of the target is significantly broader than the corresponding front images, with a strong dependence on the target thickness. These observations immediately suggest that the front side images are dominated by the plasma emission due to direct laser heating. This is consistent with the front image $Af4$ taken at a lower intensity that shows a source size of 11.4 μm, slightly smaller than the front side image $Bf4$ taken at higher intensity.

The rear side source is about a factor of 2 larger than the front side source. This is true for both the 5 μm and the 25 μm thick foil. The rear side source size becomes larger with target thickness and laser intensity.

If we consider the front and rear side emission of the 25 μm thick foil, an increase of the maximum emission by a factor of 25 can be measured (compare $Bf4$ and $Br4$). By normalizing the emission to the source size (FWHM) to get the source brilliance, the increase factor becomes about 160.

Moreover, the x-ray yield grows with increasing laser intensity. These observations are consistent with the behavior of $K\alpha$ fluorescence emission from Ti expected in these circumstances as observed in [4]. The spectroscopic analysis of these images shows that the main spectral component of the rear images is the Ti-$K\alpha$ at 4.51 keV [see Fig. 3(b)]. The electrons accelerated at the target surface will propagate through the target generating fluorescence emission along the path. At the same time the propagation of fast electrons is subject to the action of electric and magnetic fields as well as scattering processes in the material that make the electrons diffuse with a consequent increase of the fast electron beam cross section and, therefore, the $K\alpha$ source size.

Since the attenuation length of Ti-$K\alpha$ in cold Ti is 20.3 μm, the rear images observed for the 25 μm thickness targets are marginally sensitive to the fluorescence emission occurring in the first few micrometers of the fast electron propagation path as this radiation will not contribute to the rear side emission.

In contrast, the 5 μm thick foil is transparent to $K\alpha$ radiation and, to this respect, the information obtained from the 5 μm thick target is complementary to that obtained from the 25 μm thick target. Schematically, we can say that the 25 μm thick target gives the size of the fast electron beam at the output surface position. Concerning the initial size of the fast electron beam, we assume this to be approximately 3 μm, corresponding approximately to the size of the focal spot, as expected from the fast electron generation scheme based upon ponderomotive effects [16] and vacuum heating [17]. Using this values to calculate the half-aperture of the cone of fast electrons we find half-angle apertures of $\tan^{-1}\{[(\mathrm{FWHM}/2) - r]/t\} \simeq 30°$ and $\simeq 60°$ (r is the radius of the laser focal spot, t is the target thickness, and FWHM is taken from Fig. 2) for the 25 μm and 5 μm thick target, respectively.

According to these estimates, in the first few micrometers of their forward propagation, electrons are spread over a very large solid angle. After the first 5 μm, the electron beam is confined in a much narrower cone, approximately half of the initial aperture. An explanation of this behavior requires the existence of strong beam collimation fields inside the material. The existence of these fields has indeed been suggested by previous experimental studies and is predicted by numerical simulations [18–22].

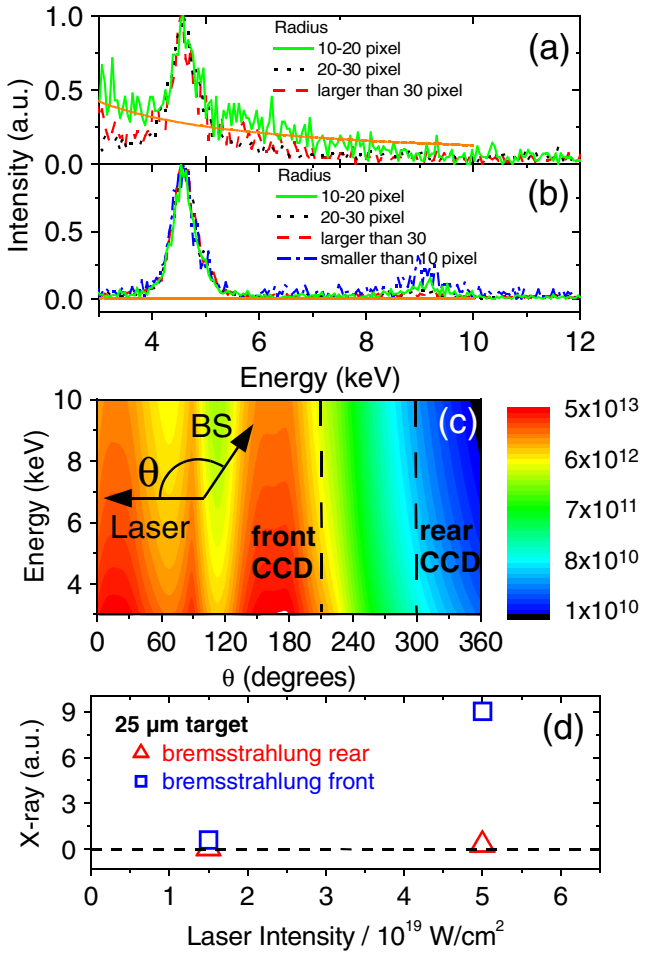

FIG. 3 (color online). Space-resolved normalized spectra extracted from the measured source for the 5 μm thick Ti foil in (a) and (b) from the front and the rear CCD, respectively. A region 80×80 pixel around the maximum emission (approximately 190×270 μm^2) was taken into account. About 110 single-shot images for each graph were analyzed. The region around the x-ray emission was divided into four parts: closer than 10 pixels to the maximum emission, between 10 and 20 pixels, between 20 and 30, and more than 30 pixels. Elliptical regions were used to compensate for the 45° angle of view. From (b) the amount of emitted photons per shot on the rear side is estimated to be about 5×10^{10}. In (c) the simulated spectrum as a function of the observation angle is shown in logarithmic scale in arbitrary units. The geometrical meaning of θ is also given: the angle between the laser direction and the bremsstrahlung (BS) emission. The two vertical lineouts correspond to the angular position of the detectors and are plotted in (a) and (b) as smooth solid lines (in orange in the online version). In (d), we plot the measured bremsstrahlung emission for the 25 μm target for the two intensities in the 3–12 keV energy range: the bremsstrahlung from the front side shows an increase by a factor 15.

We observe that the images $Cf4$ and $Cr4$, both concerning the 5 μm thin target show that, even if the target is almost transparent in the x-ray photon energy range considered here, strong differences are found in the source size, as seen by the rear CCD, which is more than 50% larger than the image seen by the front CCD.

To shed light on the data, we extracted spectra from the measured x-ray source images of Fig. 2. Briefly, the method exploits the fact that an x-ray photon, during the interaction with a CCD, frees an amount of charge proportional to its energy (see, e.g., [23,24] and references therein). If it is possible to isolate a single event, i.e., the number of pixels is much larger than the number of photons, then one can use the CCD as a nondispersive spectrometer.

We note that for the energy ranges 3–5 keV and 7–12 keV the transmission through the thin foil is higher than 50%.

The results are given in Fig. 3. We took into account here only the 5 μm target. The plots of Fig. 3 show the space-resolved emission spectra for four different regions around the maximum. In (b) the spectrum obtained from rear side source is shown: the dominating feature is the Ti-$K\alpha$ emission, with the underlying continuum below the noise level. In (a) the front side emission is reported: the spectroscopic analysis of these images is limited to the peripheral region of the focal spot, i.e., for distances greater than 10 μm from the position of maximum emission, where the single-hit spectroscopy technique can be used in our images.

This region is outside the FWHM source size. In this peripheral region, the emission is still characterized by a significant $K\alpha$ emission, superimposed on a continuum emission. As discussed below in details, this continuum may be partially due to directional bremsstrahlung from fast electrons. In addition, the front spectra have a markedly space-dependent continuum component: the outer part is mainly due to $K\alpha$ radiation, whereas the inner part shows a clear continuum component. We note here that this cannot be simply accounted for by hot plasma emission from the front side, since the target is almost transparent in a large portion of the considered spectral range, the same kind of emission should have been seen in both front and rear emission.

In contrast, different x-ray features have been seen in intensity, dimension, and spectrum from the two sides. Therefore, we are led to the conclusion that possible contribution may come from non isotropic emission of radiation due to directional bremsstrahlung from fast electrons.

The experimental results clearly show that the two aspects of the interaction that are of a primary interest for the interpretation of the experimental data are the fast electrons injected into the target and fast electrons that propagate away from the target along a direction close to the direction of specular reflection.

Finally, in Fig. 3(d), we show how the bremsstrahlung for the 25 μm target depends upon the laser intensity: in the energy range taken into account (3–12 keV), the front emission increases by a factor of 15 when the intensity is raised from 1.5×10^{19} W/cm^2 to 5×10^{19} W/cm^2, while

the increase of the rear emission is only fivefold. This plot complements in a more quantitative way the information already obtained in Fig. 2: there, the sum pictures for the 25 μm target show a clear increase of the maximum signal (MAX value) mainly on the front side as a function of the laser intensity, energy integrated. Here, we see that an increase of the impinging laser intensity by a factor of 3 results in a bremsstrahlung increase (only on the front side) by a factor 15.

In order to clarify the different aspects of the experimental findings, we used 2D PIC simulations using the EPOCH code. EPOCH is a fully electromagnetic PIC code. The target was modeled as consisting of a shelf of underdense plasma ($0.3n_{\mathrm{crit}}$ and 13 μm length) and a foil of overdense plasma ($10n_{\mathrm{crit}}$ and 15 μm thickness). The laser pulse parameters and angle of incidence used in the simulation match the experimental parameters. The simulations were run up to the point that the laser pulse had reflected from the target and had exited the underdense plasma region.

In the 2D PIC simulations, the electrons entering the target have an energy-dependent angular distribution. High energy electrons have a relatively narrow angular spread (e.g., $<30°$ FWHM at 4 MeV), but the very low energy electrons have a large angular spread ($>50°$ FWHM below 500 keV). The variation in angular spread with energy most likely gives rise to the variation in apparent beam divergence with target thickness.

Results of the 2D PIC simulations can be seen in Fig. 3(c): a significant angular dependence of the bremsstrahlung can be clearly recognized (similarly to [25] but for much lower energies). In Figs. 3(a) and 3(b) the smooth solid lines (in orange in the online version) directly compare the results of the simulations with the experimental data: whereas on the front side the bremsstrahlung presence is clearly visible, on the rear side there is almost no bremsstrahlung. The excellent agreement confirms the presence of directional bremsstrahlung.

Indeed, the most interesting result from 2D PIC simulations is that the directional bremsstrahlung, observed from the front surface, is due to electrons that are propagating away from the target, along a direction close to the direction of specular reflection. The simulations show also that electrons form a well-defined jet that is collimated by an associated, strong magnetic field (typically of the order of 2–4 kT). Since the electrons have a narrow angular spread, this leads to a directional bremsstrahlung emission. The formation of this jet is contingent on the existence of the underdense shelf in front of the target; no such jets are observed in simulations in which the shelf is absent.

In conclusion, we irradiated thin Ti foils with ultrashort, ultraintense laser pulses and we looked at the x-ray emission with an high-resolution 2D imaging system. Clear differences in intensity, dimension, and spectrum between front and rear emission could be detected, even in thin targets. The extracted space-resolved x-ray spectra concerning the front side distinctly show a marked presence of bremsstrahlung continuum which was not present in the rear side images. This effect is enhanced moving from peripheral regions towards the x-ray emission center. Relativistic 2D PIC simulations supported the analysis and confirmed the hypothesis of directional bremsstrahlung. The simulations even predict much stronger bremsstrahlung emission at well selected directions.

We wish to acknowledge the JeTi laser staff, Laser-Lab Europe, and the DFG for the support. A. P. L. R. is grateful for computational resources provided by STFC's e-Science facility, and for the provision of the EPOCH code by CCPP (particularly to T. Arber and C. Brady). The ILIL team also acknowledges financial support by the MIUR-PRIN-2007 project ''Studio della generazione di elettroni veloci [...]'' and by the HiPER Project.

*Present address: Max-Born-Institut, Berlin, Germany.
†zamponi@mbi-berlin.de
‡Present address: Laboratori Nazionali di Frascati, INFN, Frascati, Italy.

[1] A. Rousse *et al.*, Phys. Rev. E **50**, 2200 (1994).
[2] L. A. Gizzi *et al.*, Phys. Rev. Lett. **76**, 2278 (1996).
[3] A. Rousse, C. Rischel, and J.-C. Gauthier, Rev. Mod. Phys. **73**, 17 (2001).
[4] F. Ewald, H. Schwoerer, and R. Sauerbrey, Europhys. Lett. **60**, 710 (2002).
[5] T. Feurer *et al.*, Phys. Rev. E **65**, 016412 (2001).
[6] C. Reich *et al.*, Phys. Rev. Lett. **84**, 4846 (2000).
[7] F. Zamponi *et al.*, Opt. Express **18**, 947 (2010).
[8] C. Reich *et al.*, Phys. Rev. E **68**, 056408 (2003).
[9] N. Zhavoronkov *et al.*, Opt. Lett. **30**, 1737 (2005).
[10] D. Batani *et al.*, Phys. Rev. E **65**, 066409 (2002).
[11] J. A. Koch *et al.*, Phys. Rev. E **65**, 016410 (2001).
[12] F. N. Beg *et al.*, Phys. Plasmas **4**, 447 (1997).
[13] L. Gizzi *et al.*, Plasma Phys. Controlled Fusion **49**, B211 (2007).
[14] P. Köster *et al.*, Plasma Phys. Controlled Fusion **51**, 014007 (2009).
[15] F. Zamponi *et al.*, Rev. Sci. Instrum. **76**, 116101 (2005).
[16] S. C. Wilks *et al.*, Phys. Rev. Lett. **69**, 1383 (1992).
[17] F. Brunel, Phys. Rev. Lett. **59**, 52 (1987).
[18] M. Tatarakis *et al.*, Phys. Rev. Lett. **81**, 999 (1998).
[19] M. Borghesi *et al.*, Phys. Rev. Lett. **80**, 5137 (1998).
[20] A. Pukhov and J. Meyer-ter-Vehn, Phys. Rev. Lett. **76**, 3975 (1996).
[21] A. R. Bell *et al.*, Plasma Phys. Controlled Fusion **39**, 653 (1997).
[22] S. Betti *et al.*, Phys. Plasmas **16**, 100701 (2009).
[23] L. Labate *et al.*, Rev. Sci. Instrum. **78**, 103506 (2007).
[24] K. Akli *et al.*, Phys. Plasmas **14**, 023102 (2007).
[25] H. Schwoerer *et al.*, Phys. Rev. Lett. **86**, 2317 (2001).